Comparison of four mobile, non-invasive diagnostic techniques for differentiating glass types in historical leaded windows : MA-XRF , UV–Vis–NIR, Raman spectroscopy and IRT

Comparison of four mobile, non-invasive diagnostic techniques for differentiating glass types in historical leaded windows: MA-XRF, UV-Vis-NIR and Raman spectroscopy, and IRT

S. Cagno[a], G. Van der Snickt[a,b], S. Legrand[a], J. Caen[b], M. Patin[c], W. Meulebroeck[c], Y. Dirkx[d], Michaël Hillen[d], G. Steenackers[d], A. Rousaki[e], P. Vandenabeele[e,f], K. Janssens[a]

a. AXES Group, Department of Physics, University of Antwerp, Groenenborgerlaan 171, Antwerp, Belgium
b. ARCHES Group, Faculty of Design Sciences, University of Antwerp, Mutsaardstraat 31, B-2000 Antwerp, Belgium
c. Brussels Photonics (B-PHOT), Department of Applied Physics and Photonics, Vrije Universiteit Brussel, Brussels, Belgium
d. Op3Mech, University of Antwerp, Groenenborgerlaan 171, B-2020 Antwerp, Belgium
e. Raman Spectroscopy Research Group, Department of Chemistry, Ghent University, Krijgslaan 281, Ghent, Belgium
f. Archaeometry Research Group, Department of Archaeology, Ghent University, Sint-Pietersnieuwstraat 35, Ghent, Belgium

Abstract

This paper critically compares the performance of four non-invasive techniques that match the accuracy, flexibility time-efficiency and transportability required for *in situ* characterization of leaded glass windows: macroscopic X-ray fluorescence imaging (MA-XRF), UV-Vis-NIR and Raman spectroscopy, and infrared thermography (IRT). In order to compare the techniques on equal grounds, all techniques were tested independently of each other by separate research groups on the same historical leaded window, tentatively dated to the 17th century, without prior knowledge. The aim was to assess the technique's ability to document the conservation history of the window by classifying and grouping the colorless glass panes constituting the window, based on differences in composition. IRT, MA-XRF and UV-Vis-NIR spectroscopy positively distinguished at least two glass groups. MA-XRF provided the most detailed chemical information on these groups. Based on the ratio between the network modifier (K) and network stabilizer (Ca) and on the level of colorants and decolorizers (Fe, Mn, As), the number of plausible glass families could be strongly reduced. In addition, UV-Vis-NIR detected cobalt at ppm level and gave more specific information on the chromophore Fe^{2+}/Fe^{3+} ratio. Raman spectroscopy was hampered by fluorescence caused by the metal ions of the decolorizer in most of the panes, but nevertheless identified one group as HLLA.

1. INTRODUCTION

According to contemporary conservation practice, historical leaded windows are only subjected to active and passive treatment after a complete technical examination of the glass panes, the structural metal network and their (architectural) setting. This is a labor-intensive process, typically performed by visual and microscopic inspection. In a few cases, usually when deterioration or specific historical issues need to be addressed, this is complemented with analyses.

Typical analytical approaches involve sampling, after which measurements using e.g. Scanning Electron Microscopy equipped with an Energy Dispersive X-ray Spectrometer (SEM-EDS) [1], or

Laser Ablation Inductively Coupled Plasma Mass Spectrometry [2] reveal the weight percentages of the glass ingredients [3]. This usually involves point analysis on each pane, but this modus operandi is often time and capital intensive, requires interpretation by experienced staff and is always at risk of non-representativity. In addition, the extraction of sample material is subject to debate in the context of a conservation campaign and is therefore nowadays increasingly minimized in favor of non-invasive analysis performed directly on the objects. The latter raised an interest in chemical imaging techniques, such as MA-XRF, recently developed for polychrome surfaces but applicable on glass materials as well [4]. Large area imaging of entire window panels, in an almost unsupervised way, can minimize the required operator time and the risk of non-representativity, but machine time and costs can be high.

In view of these recent technical evolutions, the aim of this study is to compare the available non-invasive analytical techniques for *in situ* glass window analysis. These were assessed on the level of information that could be retrieved from a non-decorated, colorless historical leaded window dated to the 17th century, and in particular on their ability to classify glass panes in groups in function of their composition. This austere type of windows is a sizable but nevertheless largely overlooked part within the vast body of historical glass windows in monuments and museum collections. Nonetheless, the study of their materials and the production techniques can unveil a wealth of information on their history and on the craftsmen who made them. Such studies are rarely performed on large and representative sets of colorless windows, because of the time-consuming nature of this work combined with the functional character and plain appearance in comparison with more colorful and complex stained-glass windows, and . For stained-glass windows, this distinction is less intricate because later additions can often be more easily discerned by the eye, on the basis of differences in paint style or brushwork application, or differences in hue between the colored panes. For colorless, non-decorated glass panes this is more challenging since there are far less parameters that can be considered, and therefore the study remains too often limited to observation and classification by means of connoisseur's expertise.

The diagnostic methods in this study were assessed from the pragmatic viewpoint of a cultural heritage scientist. Typically operating in the field of construction yards, heritage workers are mostly interested in a swift but nevertheless truthful distinction of groups of glass types, rather than an accurate quantification of glass components, as customary in archaeological science. Therefore, next to accuracy, we focused on time-efficiency, potential *in situ* use, the ability to document entire window panels and to obtain results in an organized way. Concerning in situ use, we define it as the possibility to perform measurements outside the laboratory, at the location where the window is stored. This could be the original architectural setting of the window, a museum where it is exposed, or a conservation studio. The latter is highly relevant for measurements performed in the context of conservation interventions.

Such a classification involves recognizing non-original glass panes and estimating the number of interventions in the past, documenting thus the history of the window, which is highly relevant to design an appropriate conservation strategy.

In this paper we compare four techniques that were recently proposed for similar purposes: macroscopic X-ray fluorescence scanning (MA-XRF), UV-Vis-NIR absorption spectroscopy, Raman spectroscopy and Infrared thermography (IRT). The recent application of these techniques in this specific field are briefly described in the following paragraphs.

A mobile MA-XRF 2D scanning instrument was made available in 2011 [5] and has generated a wealth of results on flat objects such as iconic paintings (see e.g. [6, 7]), manuscripts [8], wall paintings, *etc*. MA-XRF has recently proven itself suitable for stained-glass windows screening [3] and has been applied to a real stained-glass conservation case [4]. However, it has never been tested before onto colorless windows. Since the entire surface of the window was scanned with MA-XRF and X-ray spectra were collected at each scanned pixel, comparison with spot analysis by means of portable-XRF on different glass panes (see e.g. [9, 10]) was considered superfluous.

UV-Vis-NIR absorption spectroscopy allows studying the transition metal ions or metallic particles responsible for glass coloration [11-14]. The position of the oxygen ion absorption edge in the UV-blue region (< 450 nm) is determined by its bonding state: pure glass with good UV transparency is rich in strongly bound bridging oxygen, but more impure glass with more network modifiers is richer in non-bridging oxygen. The latter is more easily excited and shifts the absorption edge towards longer wavelengths [15]. In this way, spectra of glass of different composition families can be distinguished, and, next to the color coordinates, information can be obtained on the redox state of production of the glass, i.e. the atmosphere of the furnace and its oxidation degree [16, 17].

Raman spectroscopy is widely applied in glass archaeometry and conservation studies, (e.g. [18-20]), also with non-invasive, portable setups [21-23]. In man-made glass, additions such as flux and colorants (alkali metal earths or metal oxides) alter the linkages in the silica network replacing the oxygen atoms connecting the SiO_4 tetrahedra by non-bridging oxygens [18-20]. By studying the Si-O bending (at around 500 cm^{-1}) and stretching (at around 1000 cm^{-1}) modes of the SiO_4 tetrahedron and the A_{500}/A_{100} ratio, glass type and degree of polymerization can be identified [18, 19, 21].

Infrared thermography has been used for a variety of art inspection and conservation cases [e.g., 24, 25], including a few applications on glass materials, mostly stained-glass windows [26-30]. The technique has proven effective in mapping the surface alteration features of archaeological glass [26], and in distinguishing e.g. soda-lime base glass and applied lead-glass paint in stained glass windows due to differences in heat accumulation [30].

2. MATERIALS AND METHODS

2.1. The window

The small window investigated in this study (Figure 1) is part of the private collection of co-author Joost Caen, who received it from a German collector. According to its former owner, the panel originates from Westphalia, North-Western Germany. The object was in bad condition, as several pieces of glass were broken or missing. The frame was damaged and the glazing bars were not well connected to the lead profiles of the panel. The glass panes exhibit typical whitish glass corrosion products in a streaky pattern on the interior side. Visual observation and style comparison pointed out that the small window can be dated to the 17th century [31]. The appearance of the panel is typical for that region but was also popular in the Northern Netherlands during the same period. However, the rectangular glass panes were usually significantly larger in the Northern Netherlands.

The panel underwent a conservation-restoration treatment: broken glass was bonded with epoxy resin; lead profiles, bars and frame were treated and, most importantly, infills with recuperated old

similar-looking glass were inserted. This treatment resulted in a panel that looks visually homogeneous, containing only historical glass, but not from the same period, making it a suitable subject for this comparative study. The glass displays a light greenish hue that is not uniform for all panes as can be seen in Figure 1.

2.2. MA-XRF

The window was analyzed in reflection mode from the exterior side by means of the MA-XRF scanning instrument version I (Figure 2), built within the AXES group of the University of Antwerp. The scanner consists of an XRF measurement head mounted on a software-controlled X-Y motor stage with a travel range of about 60 x 57 cm (h x v). The measurement head was equipped with one Vortex EX-90 SDD detector positioned at a 20° angle with respect to the incident X-ray beam. The X-ray source is a XOS 50W Rh anode tube. The diameter of the primary beam was reduced to a focal spot of 200 µm by implementing a polycapillary X-ray lens.

MA-XRF scans were performed by sweeping the measuring head systematically over the glass surface, respecting a stable distance of ca. 2.2 cm in between the edge of the measuring head and the panel. For each pixel in the scanned area, an XRF spectrum is collected. From these spectra, XRF maps are created for each element detected, after a spectral fitting process [6]. The resulting maps, shown in Figure 6, are gamma/contrast adjusted for better reading, carefully avoiding the creation of artefacts. A step size of 800 µm and a dwell time of 500 ms were used for this scan, resulting in a relatively slow scan speed, to improve the statistics. In this way, an area of 431 by 387 pixels was covered in a scan time of 24 hours.

The MA-XRF setup is transportable and can be used at the location where the objects are stored or restored. In principle, performing in situ scans in an architectural setting on scaffolding is feasible with this homebuilt setup as well, as was recently demonstrated for the study of wall paintings (results forthcoming), but requires supporting structures that allow for safe and stable positioning of the equipment and the absence of physical obstructions that can hamper the movement of the measuring head. Thus, this would exclude *in-situ* analyses of very large windows. In this case the window was positioned on a dedicated support in a conservation studio for the entire duration of the measurements, while the measuring head moved across the entire surface, as shown by Figure 2.

2.3. UV-Vis-NIR spectroscopy

The measurement set-up is shown in Figure 3. We employed a DHS-BAL deuterium lamp combined with the Avalight-HAL halogen source and an Avaspec-3648 and AvaSpec256 optical spectrum analyzer from Avantes. An optical density filter with OD value 1 was placed in front of the halogen source in order to match the dynamic range of both light sources. The small dimensions of the equipment allow carriage in one piece of luggage and facilitates transport e.g. in airplane. When working in situ, it is possible to use portable batteries or a power supply. To set up the equipment it is only necessary to delimitate a small working area in the dark with a table to support the piece horizontally. Setting-up the equipment takes approximately one hour but it is at the same time possible to start selecting the samples or points to measure. Afterwards, recording the spectra is very fast (3 minutes per selected point). For this study, it took an afternoon to install the setup, prepare the points and to measure the thickness of each glass piece (with an Olympus ultrasonic test gauge) and to record the spectra of the 26 glass pieces composing the window.

Optical transmission spectra were recorded in the spectral region between 250 nm and 1750 nm, with a spectral resolution of 1.4 nm (Avaspec-3648) and 4 nm (AvaSpec256). The light emitted by the light source is focused to a spot size of 1.5 mm on the panel. All the transmitted light is captured by an integrating sphere, which is connected to the optical spectrum analyzer. This implies that only translucent and thin parts up to 3.5 mm can be studied with this technique [17]. Moreover, dirty, corroded or weathered parts should first be cleaned, envisioning a clean sample at the position of the light spot. Although the window under study showed corrosion at various places, a clean spot was found for each pane.

2.4.Raman spectroscopy

All measurements performed with the portable EZRaman-I dual analyser (TSI, Irvine, USA). This dual laser spectrometer allows the recording of spectra in spectral ranges of 100–2200 cm^{-1} and 100–3100 cm^{-1}, for the a red diode laser (785 nm) and a green Nd:YAG laser (532 nm), respectively. The Raman system uses long fibre optics cables to measure the artefacts/samples, with the option of three interchangeable lenses per wavelength and is coupled with a thermo-electrically (TE)-cooled (−50°C) CCD detector. The entire system together with the laptop controlling the measurements is built-in a suitcase (Figure 4).

In this study, the green Nd:YAG laser (532 nm) was employed. The long fibre optics probehead was positioned and focused on the surface of the subject under study via an articulated arm and the standard lens (STD) was used having a focal length at 8 mm. The laser power was kept under 50% (lower than approximately 26 mW) of the total laser power of the system (maximum power 50 mW). The experiments were conducted in darkness to avoid the interferences of the environmental signal and ambient light. The number of accumulations and measurement time varied between 100 to 400 acc of 20 to 150 sec and adjusted per point to obtain spectra with good signal-to-noise (S/N) ratios. The Raman spectrometer was calibrated with sulphur, epsilon-caprolactone (Acros Organics), cyclohexane (Kaiser), polystyrene pellets (Aldrich), and acetonitrile (Panreac)/toluene (UCB; mixed in 50/50 volume%) [32, 33].

Calibration and acquisition of data was performed with an in house software while post data treatment was performed by using Thermo Grams/AI 8.0® suite software (Thermo Fischer Scientific), by applying a linear baseline correction using 4 segments at approximately 200 to 700 cm^{-1}, 700-800 cm^{-1}, 800-1250 cm^{-1} and >1250 cm^{-1}. The Raman spectra were treated as described in Colomban, 2003 and Colomban et al., 2006 [18, 19].

2.5.IRT

Active thermographic experiments were performed by generating small thermal differences in the window by applying external heat for 2 min, followed by a 3 min cooling-down process. The ensuing thermal anomalies were investigated by acquiring a series of thermograms at a frame rate of 10 Hz [34-37].

As illustrated by figure 3, the experiments were performed with the exterior side of the window facing the camera while the panel was heated using two 500 W halogen lamps from the exterior side. The lamps were positioned symmetrically with respect to the camera (Figure 5) and at a distance of 0.80 m, measured from the sides of the window frame. The camera was positioned at 0.8 m from the center of the window. A FLIR X6540sc actively cooled, thermal camera, which has a thermal sensitivity of <25 mK (typically 18 mK) and a resolution of 640×512 was used [38].

A Q L1009 25 mm f/2 lens was used, which has a spectral range of 3.5–5 μm and a Field of View (FOV) of 21.74° × 17.46°.

3. RESULTS AND DISCUSSION

3.1.MA-XRF

In this section, we discuss the elemental distribution maps (Figure 6) that were obtained after spectral deconvolution (fitting) of the data cube containing the X-ray spectra collected at each pixel. The pixel intensities in these contrast maps are rendered in grey values and are relative indications of the concentration of a chemical element. In particular, black pixels imply that a given element was not detected in the corresponding volume on the surface, while brighter tones indicate a proportional increase of the net peak surface of the emission lines of a particular element. Next to these distribution images, the pixel intensities are also shown as bi-plots in Figure 9, permitting to spatially assess the ratio of two elements. By assigning user-chosen colors to the identified clusters, and coloring the pixels of an elemental map accordingly, grouping of glass panes can be visualized in false colors. Although XRF spectra of individual pixels are not shown, the average spectra of all glass groups identified in the window, obtained from all pixel spectra assigned to a group as described in Table 1, are presented in Figure 7 (for the main glass group identified in this study) and Figures S1-S3 (for the other groups) in the Supplementary Information. As discussed in the next few paragraphs, a careful assessment of these images permits grouping the glass panes and, to some extent, even attributing these groups to established types of historical glass.

For MA-XRF, the glass types are grouped based on the presence and relative concentration of chemical elements in the separate glass panes. This elemental signature is determined by the (proportional) introduction of raw materials into the glass batch, i.e. the type of silica source, flux, network stabilizers and other additives such as chromophores.

The glass type classification flowchart by Schalm et al. [1, 4] in Figure 8 indicates the glass families that can potentially occur in this window, based on its proposed provenance. On the basis of its composition, the window glass produced and traded in the Low Countries and surrounding areas (e.g. the Rhine area in Germany) from the 16th century to present can be categorized as: potash glass, high-lime low-alkali (HLLA) glass, lead glass, vegetable ash soda glass and synthetic soda glass [1, 4]. Further information on categories of historical window glass in other contexts can be found elsewhere [1, 9]. In addition, Figure 8 demonstrates that the hierarchical classification is based on the chemical elements Na, K, Ca and Pb. However, for MA-XRF, low energetic fluorescence radiation, such as the Na emission lines, are readily absorbed by the ambient air on its path to the detector. Therefore, for MA-XRF analysis, only the K, Ca and Pb distribution maps can be employed to classify glass. Two glass families can be immediately excluded: lead glass and synthetic soda glass, containing no potassium. As illustrated by the average spectra in Figure 7, S1-S3, the enhanced contrast Pb-map shown in Figure S5, and the average Pb intensities shown in Table 1, only minor Pb signals were detected in the glass, therefore the presence of lead glass, with a lead content exceeding 14%, can be ruled out. Synthetic soda glass could occur in case of replacements with modern times glass. Nevertheless, although Na is not detectable, such infills with synthetic soda glass, can be indirectly excluded. This high purity glass, industrially produced from the late 18th century onwards, is characterized by no, or a very low K content, typical below the detection limits of XRF in ambient air [4]. The detection of K in all panes, therefore seems to exclude the presence of this modern glass (see Figure 5 G).

The K and Ca distribution maps, shown in Figure 6 G-H, promptly reveal two types of glass upon inspection. Three glass panes stand out in the elemental images by a substantially higher potassium and a slightly lower Ca intensity. In view of its high-potassium content, and, according to the flowchart, if less than 4.5% Na was present, this glass would be situated either in the HLLA (containing 3-10% K and 15-20% Ca) or the potash glass (containing 11-17% K and 7-16% Ca) categories, while if more than 4.5% Na was present, it would most likely fit into the mixed alkali glass group (containing on average 3% K and 7% Ca) [1, 9] of Figure 8.

As the flowchart proposes a further distinction based on the K/Ca ratio with HLLA below and potash glass above the threshold value of 0.6, an attempt was made to discriminate between these types. As K and Ca are adjacent elements in the periodic system, their characteristic X-rays undergo similar attenuation phenomena and by consequence their fluorescence ratios can be compared even in these non-optimal conditions. In addition, any artefacts in individual spectra caused by e.g. local surface effects are statistically evened out by the large amount of analyzed pixels per glass pane. The ratio between K and Ca reveals an intensity ratio of approximately 0.33 for the three potassium rich panes, which would allow a classification as HLLA. Moreover, this value is close the average ratio of 0.36 reported in literature for HLLA window glass of the 16-17th century [1] and of 0.28 for HLLA window glass of the 17th century [9]. Mixed alkali kelp glass, an early industrial glass produced from the end of the 17th century to the early 19th century with the introduction of both K and Na as alkalis, has an average ratio of 0.47, and a lower iron content than HLLA glass (see further) [9].

As illustrated by Figure 9 A, three groups of glass emerge in the K/Ca biplot, along three different correlation lines. The three aforementioned potassium rich panes stand out clearly and are color-coded in *green*. However, the majority of the panes appears to belong to the *yellow* group. These panes exhibit a similar, but less intense K signal in the corresponding MA-XRF map. Here, the absence of information on the Na content renders the classification to a glass family more challenging. The K/Ca ratio is approximately 0.10, well below the previous group, and leaves a few possibilities open. If the Na content was low, the glass from this group could belong to a more lime-rich type of HLLA, which occurred frequently in the Low Countries until the 18th century, containing on average 3% K and 15% Ca (K/Ca ratio around 0.2) [1], where the depletion of K due to glass alteration could account for the lower K/Ca ratio (see further). If Na was abundant, instead, the *yellow* group could fall within the aforementioned mixed alkali group, but the K/Ca ratio could also approach that of certain early types of soda glasses with potassium impurities (e.g. 0.5% K and 5% Ca), reported in the 19th century in England [9]. However, the K intensities detected in this glass panes (see the average spectrum in Figure 7) would seem to exclude such a low K concentration in this group. In conclusion, an unambiguous classification of these panes will require further analysis (of samples).

Interestingly, the bi-plot reveals a third cluster, color-coded in *red* that consists of three small panes with an even lower K/Ca ratio of 0.06 on average. One of these is not a full pane, but rather a *fragment* that serves as an infill for a lacuna. A second, *triangular* shaped pane seems to display an intermediate composition with a substantial number of pixels belonging to the *yellow* and the *red* group. This ambiguity calls for a confirmation of the aforementioned classification by considering bi-plots of other elements, preferably with higher atomic numbers. Being more energetic, their X-ray emission is less attenuated by potential artefacts at or just below the surface that might have a local shielding effect on the emitted radiation. Care must be especially taken with interpreting the K/Ca ratio as atmospheric weathering of glass is known to cause a surface

depletion of alkalis (K and Na) and/or the formation of Ca-rich deposits (carbonates, sulfates, etc.) [39, 40]. The window under study shows whitish spots and streaks typical of corrosion. However, in this case, the defect is not expected to have a critical impact on the statistical grouping of the panes as (a) the spotty pattern does not show up macroscopically in the Ca and K maps in Figure 6 G-H, except for a marginal part of the central glass pane, as shown with greater detail in Figure S4, (b) the deposits cover a comparable low percentage of the surface, and (c) the deposits are relatively uniformly present on all panes. For the latter, this implies that the signals from all panes are more or less affected in the same way. However, it is clear that care should be taken, certainly for windows that are subject to heavier corrosion.

The Fe/Mn bi-plot (Figure 9 B) confirms the K/Ca-based results by revealing the same three groups, consisting of the exact same panes. One exception is the 'indecisive' *triangular* pane that is here positively added to the largest *yellow* group. The three *green* panes stand out from the rest by an elevated iron and lower manganese content, but this is discussed in more detail further in the text where the chromophores are addressed.

As mentioned earlier, the Sr/As bi-plot are of special interest as these energetic fluorescence signals (Sr-Ka=14.16 keV and As-Ka=10.54 keV) are the least attenuated by potential artefacts on their path to the detector. However, this also implies that the detected signals can stem from deeper inside the sample [3-6]. In this way, the glass thickness might start influencing the detected intensities as the maximum information depth for these higher Z elements with this specific set-up (i.e. for As-Ka $d_{99\%}$ = 0.99 mm and for Sr-Ka $d_{99\%}$= 2.28 mm) come close to the typical thickness of the glass sheets produced in the 17^{th}–18^{th} century (2-3 mm), as explained elsewhere [3]. Similar to the K/Ca bi-plots, in Fig. 9 C three pixel clusters emerge. However, there are two notable differences: the small pane in the upper left corner and the aforementioned infill *fragment* are here added to the *green* group, while, here shown in *blue*, a pane that was part of the largest *yellow* group in the previous bi-plots is here linked with the 'indecisive' *triangular* pane, that contains both *yellow* and *red* pixels in the K/Ca plot. Upon considering the As-K and Sr-K MA-XRF maps in Figures 6 F and 6 J, the pixels of these two panes do stand out with a brighter grey value. While the higher intensities detected for these heavier elements could be due to a higher thickness of these particular glass panes, rather than a compositional difference, the glass thickness measurements performed in the UV-Vis-NIR session (see further) clarified that glass thickness in this window varies independently from the glass classification.

In conclusion, taking into account (a) the potential ambiguity of the Sr/As plot, (b) the supposedly trivial influence of the corrosion on the K/Ca plot and (c) its validation by the Fe/Mn plot, we assess the grouping by the K/Ca plot as the most reliable, while the indecisive triangular pane and the larger pane associated with it by the Sr/As plot (Figure 9 C) remain in limbo and could be considered part of a further group.

Since the window is composed of colorless glass, none of the panes show a signal that is indicative for the intentional addition of typical glass colorants. However, as illustrated by Figure 6, three glasses exhibit a higher level of iron (figure 6 C) and to a lesser extent of cobalt (Figure 6 D). Upon careful visual inspection, these glass panes also display a slightly greener hue, typically associated with an impure silica source containing traces of Fe^{2+} and Fe^{3+} metal ions. In order to counteract this unsolicited yellow green color, glassmakers often added manganese to the melt as a decolorizer. Whereas Mn^{3+} has the ability to produce a purplish color under the right furnace conditions and in sufficient quantity (typical more than 0.5 wt. %), in the presence of Fe^{2+} it will

reduce to colorless Mn^{2+} while oxidizing the iron to Fe^{3+}. The latter gives rise to a yellow color, but the Fe^{3+} ions have a substantially lower tinting strength, resulting in a less colored glass [16, 41]. As illustrated by Figure 6 E, Mn was detected in most of the colorless panes of the window under study, suggesting the employment of a decolorizer. This underpins the aforementioned excluded presence of industrial-age glass as this is manufactured with high purity raw materials, free of Mn contamination and without the need to add de-colorizers in its production process. The three greenish panes (*green* group) are significantly poorer in Mn, while at the same time richer in Fe, suggesting that this was a more economical 'common' glass for which less pure ingredients were employed while a decolorizer was cost-cut.

From the 18th century onwards, and typically up until the 19th century, also arsenic was used as decolorizer and as a refining agent for removing gas bubbles [42]. As expected, the greenish glasses contain no or very little arsenic, while the others, but two (top left and mid-bottom pane) show presence of As. The presence of different types of decolorizers (Mn and As) in this window can also be used as a discriminant of glass types. In literature, Mn presence centered at levels above and below 0.15 wt. % was measured in HLLA glass in English windows of the 16-17th century [9], and the addition of both Mn and As to improve the appearance of crown glass is mentioned in British recipes of the early 19th century [43].

Next to the glass constituents, non-glass materials show up in the images as well. In particular, the XRF maps of Pb and Sn (Figure 6 A-B) selectively plot the lead came network and soldering joints. In this way, the lead and tin images can also be employed as a by-product of the experiments to document potential discontinuities in these structural components before and after treatment. As such, the MA-XRF maps can serve as an unbiased supplementary to the visual observations and photographic material made by the conservator and can objectively testify the post-procedure quality in the conservation report. In this case, the lead network and the junctions are free of structural gaps.

Summarizing, with MA-XRF the glass panes could be classified in 4 groups, as described in Table 1. These are the *yellow*, *green* and *red* glass groups identified in Figure 9 A-B, to which a fourth group (*blue*) was added, constituted by the two indecisive panes standing out mainly due to their higher Sr and As intensities (Figure 9 C). In Table 1, the peak intensities of the four groups are shown for a set of seven diagnostic elements (K, Ca, Mn, Fe, As, Sr, Pb). For each group, these intensities were calculated from the average spectra (Figure 7, S1-S3) obtained from all individual pixel spectra. Pixels neighboring the lead came network were excluded.

3.2.UV-Vis-NIR spectroscopy

UV-Vis-NIR spectroscopy uses the said presence of coloring iron ions, originating from the sand sources, to group glass. In silica glasses, iron is stable in the two ionic forms Fe^{2+} and Fe^{3+}. The divalent form (Fe^{2+}) absorbs in the near-infrared part of the electromagnetic spectrum with a broad absorption band tailing in the visible part of the spectrum. This imparts a blue color. For silica glasses the band is situated close to 1100 nm [44]. Trivalent iron (Fe^{3+}) has narrow weak absorption bands close to 380, 420 and 440 nm leading to a pale-yellow color. Observation of the appearance/absence of these bands and their strengths unveils information about the glass composition and technology. This is because the iron redox ratio (Fe^{2+}/Fe^{3+}) is influenced by the used raw materials as well as by the furnace conditions.

Analyzing the spectral shapes of the recorded spectra by calculating the L*a*b* color coordinates (for the illuminant D65) (Figure 10 A), together with the UV absorption edge and the absorbance at 1100 nm (see Figure 9 B), allows concluding that the panel shows the presence of five different glass groups (Table 2). The first group is largely overlapping with the MA-XRF *yellow* group; the second consists of two panes that were assigned to the *yellow* group by MA-XRF, the third and fourth groups coincide with the MA-XRF *green* and *red* groups, while the last group, made of the upper fragment of a re-composed pane only, was not recognized by MA-XRF. The latter fragment was not analyzed with MA-XRF, because the measuring head could not reach the uppermost centimeters of the window due to the protruding frame. In this way, this practical shortcoming underlines how the (architectural) setting of a window can limit the in situ scanning.

The differences in overall spectral shape are not only originating from differences in iron ion concentrations. The absence or presence of the three characteristic successive absorption bands close to 530, 594 and 650 nm of tetrahedral coordinated Co^{2+}, and their potential strength, contribute to the identification of the different glass groups as well. For two of the five groups for example, the presence of cobalt is clearly visible (Group 1 and 2). Both groups have clearly different cobalt concentrations (Figure 10 C). Glass thickness is rather variable across the panes (from 0.6 to 2.2 mm) and it does not depend on the classification in groups mentioned above.

In this stage, the groups cannot be assigned to specific glass families yet. Past research defined the optical measures that allow the identification of sherds to Late Antique glass [14]. Ongoing work (forthcoming) is researching the optical signatures of post-medieval glass families, allowing to link to each of the identified groups a specific glass family, based on various optical parameters and the global shape of the spectra collected on stained-glass from the Low Countries.

The groups identified in the window can be defined as shown in Table 2, where, also by comparison with spectra of known glass compositions [45], possible attribution to glass families (HLLA and mixed-alkali) are proposed for the first three groups. Representative spectra for all groups described in Table 2 are shown in Figure S6 in the Supplementary Information.

3.3. Raman spectroscopy

Raman spectra were collected from all the panes of the glass window. However, for most of the glass panes the data retrieved excess fluorescence. Fluorescence can be caused by presence of several metal ions (e.g. manganese, which was detected in most of the panes by MA-XRF) in the glass matrix and impedes the identification of the glass matrices. These panes, for which the glass type could not be determined, are all part of the *yellow*, *blue* and *red* MA-XRF groups. MA-XRF determined in all these groups a Mn content (Table 1), and this could be one of the reasons of the excess fluorescence.

For four glass panes, instead, spectra without excess fluorescence were obtained. These were: the three panes part of the *green* MA-XRF group, and the corner fragment of a re-composed pane (*purple* UV-Vis-NIR group). In Figure 11 the pane locations are shown and the raw and the baseline spectra are plotted.

The peak fitting was achieved by using Gaussian shapes for the glassy matrix. For the Si-O stretching range at approximately 1250 to 700 cm^{-1} five bands were fitted and an equal number for the Si-O bending region at approximately 700 to 200 cm^{-1}. The fitting of the Si-O stretching and

bending region is demonstrated for pane A in Figure S7 in the Supplementary Information. From the peak parameters collected in this way, the polymerization index $I_p = A_{500}/A_{100}$ was calculated.

The four panes fall within two groups in terms of I_p: (1) the *purple* fragment has an I*p* of 1.89 and (2) the *green* panes show similar I_p values of 2.46, 2.49 and 2.67. Polymerization indexes between 1.3 and 2.5 imply Ca-based glasses, while I_p higher than 2.5 are typical of K-based glazes and glasses [18, 19].

Therefore, the *purple* fragment is situated well within the Ca-based glass family, which could be compatible with a potassium poor HLLA glass [1, 9]. The *green* group panes, instead, are situated at the border between Ca-based and K-based glasses, which could imply a potassium-rich HLLA glass [1, 9], consistently with the detection of abundant K by MA-XRF in these panes (*green* group), with an average 0.33 K/Ca ratio (Table 1). This is a further element indicating that the *green* group is HLLA glass, rather than the other plausible families defined by MA-XRF (see Table 1 and Table 2). Finally, an estimation of the firing temperature can be made through the polymerization index. All four panes are estimated to have had firing temperatures around 1000°C to 1400°C [18, 19].

While MA-XRF signaled a relatively high potassium content in the *green* group, but not allowing an equivocal classification due to missing information on its sodium content, Raman spectroscopy could *positively* identify it as an intermediate between a K-based and Ca-based silicate matrix. However, the remaining glass groups (excluding the *purple* fragment), could only be grouped *negatively* and without further distinction by Raman spectroscopy, due to excess fluorescence.

3.4. IRT

In contrast with the aforementioned methods, IRT does not distinguish compositional glass types based on a different spectral signature but on their thermal behavior. By consequence, it cannot be excluded that glass panes with a deviating composition exhibit a similar photothermal emission upon heating. In order to assess if the difference in photothermal response is significant enough to allow for glass type grouping, active thermography was performed on this window. In order to obtain images with sufficient spatial resolution, the upper and lower part of the window panel were imaged separately. As shown in Figure 12, the resulting images have one row of glass panes in common by way of overlap. The window was imaged in four modalities: in reflection and in transmission mode, and at two times: immediately after heating/before cooling (t=0) and during cooling (t=2 min). In contrast with the reflection mode, the transmission images show degradation on the glass surface, while exhibiting less contrast between the different glass panes. Therefore, it seems that reflection mode measurements are better suited for this kind of investigation.

Inspection of the thermograms shown in Figure 12 immediately reveals that two types of glass are present. Both in reflected and transmitted mode, the three panes that were identified as the *green* group by MA-XRF seem to heat up faster and cool down slower than the other panes, indicated by the green dashed line in Figure 12 A. This increased heating might be due to higher heat absorption due to their different chemical composition than the rest of the panes, which was earlier demonstrated by MA-XRF and UV-Vis-NIR spectroscopy. In addition, the thermograms recorded during cooling (t=2 min), show additional groups. First, two small panes in the upper right corner stand out in as indicated by the red dashed line in Figure 12 C-D. Only the *triangular* pane surfaced

in the MA-XRF measurements as part of the *blue* group with higher As and Sr signals, while UV-Vis-NIR spectroscopy did not distinguish it from the surrounding panes. Second, four panes on the right-hand side, indicated by the yellow dashed line in Figure 12 C-D, seem to cool down faster than the others, although this group stands out less strongly than the aforementioned group. Remarkably, neither MA-XRF nor UV-Vis-NIR identify a similar group, suggesting that the observed cooling differences might be ascribed to e.g. variations in glass thickness or heat dispersion by other components of the window (e.g. lead network and frame), rather than to a compositional discrepancy.

In summary, two types of glass can be distinguished with certainty by IRT: (1) the three greenish panes (MA-XRF *green* group), which clearly heat up and cool down faster than the others; (2) most of the remaining glass (MA-XRF *yellow*, *green* and *blue* groups). A third and a fourth group show up exclusively during cooling, but only the small triangular pane was confirmed by the spectral techniques to have a different composition. Finally, for the two re-composed panes in the upper and lower row of the window, only the smaller upper fragment can be distinguished from the remainder by IRT, while for the larger pane only displays a faint discontinuity along the joint, but no difference between the two glass pieces who compose it (see IRT-Raman scheme in Figure 13).

3.5.Assessment of the four techniques

All four techniques were able to distinguish two major groups of glass (*green* and *yellow*) in a consistent way, as well as the re-composed panes made by two different pieces of glass. A visual comparison of the results of the techniques is shown in Figure 13. It is striking how the independent attribution of glass panes to groups largely overlaps, but with minor differences.

For all techniques, fast and non-invasive measurements are possible also on scaffolding positioned near *in-situ* preserved windows. This is especially the case for UV-Vis-NIR, Raman and IRT, but less for MA-XRF which is more suitable for imaging experiments in a conservation studio, after removal form their architectural setting. Thus all methods have the potential to greatly reduce the number of samples required to gather comprehensive information on glass composition. For instance, for this case, only 4-5 micro-samples (i.e., one per group) would be needed, instead of 26 (i.e., one per glass piece). Moreover, these few samples can be selected based on objective and measurable properties, rather than by using random or subjective sampling strategies.

The main advantage of MA-XRF in this context is that it provides direct, albeit not quantitative, information on the chemical elements. If only classification of panes is desired, it can be obtained relatively quickly, once the data is collected, by making use of element bi-plots and false color maps, as demonstrated in Figure 9. If a more refined classification of the composition classes is desired, element distributions and relative XRF intensities can be compared with literature, while being aware of possible errors due to e.g. glass alteration.

Concerning disadvantages of MA-XRF, the absence of information on low Z elements such as Na and Mg due to the analysis in ambient air is an issue limiting the glass type attribution. The relative long measurement time (24 h) for this experiment can be further reduced by lowering the resolution and thus the scan speed, since high-resolution maps are not required for this type of objects. Most of the experiment time consists of automated, unsupervised operation during which the operator can perform other tasks. Unlike the other three techniques, measuring with ionizing radiation

implies that safety precautions must be taken and the scanner and immediate surroundings must be clearly delimited.

The main advantages of UV-Vis-NIR absorption spectroscopy is the fast installation of portable and rather small equipment and the limited safety precautions required. The equipment also allows manipulation and flexible movement of the setup in order to reach specific locations which might be hidden by architectural/structural features. The evaluation of the results is quite straightforward and it is possible to recognize the presence of specific ions (Fe^{2+} and Co^{2+}) or metallic inclusions in the glass matrix as copper from the spectral shape. The method is able to recognize glass from the same batch by studying specific absorption bands, the coloring agents and recycling traces (as ppm levels of Co), but the exact glass family cannot be identified (yet) [46]. With the color coordinates, an objective description of an object can be proposed and the presence of thin paint layers and alterations not visible by naked eye can be highlighted. As shown earlier, this technique can provide first-line insights in the adopted production technology of bare glass [16], and glass windows can be authenticated [12].

A disadvantage of UV-Vis-NIR absorption spectroscopy is that the measurement is limited by the presence and the thickness of the lead or wood profile, which should not exceed the distance between the focusing lens and the integrating sphere. Other limitations of the methods are the necessity to work with translucent and thin (up to 3.5 mm) material, which can be a problem in presence of relevant amount of glass alteration, dust, or dark paint layers (such as grisaille). Even though reflection spectroscopy can overcome this disadvantage, the thickness of the object (measured with a Vernier or an ultrasonic thickness gauge) must be known and the operator must work in a dark environment.

Unlike laboratory-based micro-Raman spectroscopy, portable Raman spectroscopy does not require small sample sizes to fit under the Raman microscope, and is therefore a completely non-invasive and non-destructive technique for characterizing *in situ* glass windows, as proven for stained-glass windows [23]. Setup and data collection are rather quick.

The main disadvantages concern the requirement of complete darkness for measurement, and potential excess fluorescence due to the presence of manganese or other metal ions, which prevent further processing of the spectra. Data analysis requires knowledge of the literature and expertise on the specific material under study (ancient glass in this case).

The advantages of IRT are the very compact set-up, made only of two lamps and a camera, and the quick measurement time of only 5 minutes. When considering also the set-up and data analysis time, only a few hours are required in total. It appears that thermograms recorded (a) in reflection mode, (b) with the exterior/non-corroded side of the window facing the camera, and (c) before cooling (t=0) are more beneficial for glass classification as compared to images in transmission and during cooling. For (a) and (b) this is due to an elevated contrast between the glass types and less impact by corrosion products. For (c): although thermograms recorded during cooling reveal more groups, the variation seems due to an enhanced heat discharge that is caused by parameters unrelated to the glass composition.

However, more research is necessary to identify such parameters and quantify their effect. Nevertheless, IRT seems a promising technique for swift recognition of glass types. Some notable differences with the spectral techniques suggest that care should be taken with differences in thermal behavior attributable to morphological aspects or other components of the leaded window.

Further processing of the data, such as application of clustering algorithms, might result in more reliable results, based on the entire time sequence of recorded thermograms [34].

4. Conclusions

The aim of this study was to assess to what the extent the techniques are able to visualize compositional differences between glass panes, indicative of the introduction of different glass types during various interventions. In what is its first application on a colorless historical leaded window, MA-XRF was able to distinguish the two main groups of glass in function of their potassium levels, pointing to a different type of flux used. While a group made of three panes (*green* group) has a compatible composition with the attributed 17th century date of the window, most glass panes seem to contain arsenic, which is rather indicative for glass production from the 18th century onwards. The main asset of MA-XRF is its semi-quantitative aspect that allows comparison with compositions published in literature, independent from prior acquisition of a database of measurements with the same instrument.

The groups identified by UV-Vis-NIR spectroscopy match the MA-XRF groups very well, with minor exceptions. From this study it emerges that MA-XRF and UV-Vis-NIR spectroscopy could complement each other very well in studies of window glass, and could thereby improve their ability in glass identification, especially if complemented with quantitative data as a reference set.

Raman spectroscopy has proven its potential in glass type identification by means of the polymerization index, confirming the classification obtained by the other methods for part of the glass panes. Its applicability to this case study has been limited by the fluorescence recorded in the glass spectra, which did not allow to extract glass type information for the majority of the panes, probably due to manganese. This is a substantial limitation for colorless glass identification, as Mn is often present as decolorizer. However, fluorescence itself can be an indirect indication of presence of manganese in the glass, as confirmed by MA-XRF results.

IRT has proven capable of distinguishing the two main glass compositions and the split panes. However, the disturbances due to thermal dispersion did not allow to push the classification further. Due to its low cost and rapid measurement, IRT can be a valid preliminary characterization technique, calling for more specialized techniques, when interesting features should emerge.

Finally, this comparative analytical study of colorless window glass indicates that the methods under study have the potential to reveal a larger diversity in historic window glazing than currently reported by glass conservators and connoisseurs.

Acknowledgements

This research was supported by the Baillet Latour fund (AXES and ARCHES) and by the Belgian Science Policy Office supported through contract no. BR/175/A3/FENESTRA (B-PHOT). Anastasia Rousaki acknowledges the Research Foundation–Flanders (FWO-Vlaanderen) for her postdoctoral grant with project number: 12X1919N and thank Mafalda Costa for her input on determination of glass matrices via Raman spectroscopy.

References

[1] O. Schalm, K. Janssens, H. Wouters, D. Caluwé, Composition of 12–18th century window glass in Belgium: Non-figurative windows in secular buildings and stained-glass windows in religious buildings, Spectrochimica Acta B 62 (2007) 663-668.

[2] B. Wagner, A. Nowak, E. Bulska, J. Kunicki-Goldfinger, O.Schalm, K. Janssens, Complementary analysis of historical glass by scanning electron microscopy with energy dispersive X-ray spectroscopy and laser ablation inductively coupled plasma mass spectrometry, Microchimica Acta 162 (2008), 415-424

[3] G. Van der Snickt, S. Legrand, J. Caen, F. Vanmeert, M. Alfeld, K. Janssens, Chemical imaging of stained-glass windows by means of macro X-ray fluorescence (MA-XRF) scanning, Microchemical Journal 124 (2016) 615–622

[4] S. Legrand, G. Van der Snickt, S. Cagno, J. Caen, K. Janssens, Ma-Xrf Imaging As A Tool To Characterize The 16th Century Heraldic Stained-Glass Panels In Ghent Saint Bavo Cathedral, Journal of Cultural Heritage 40 (2019), 163, 168

[5] M. Alfeld, K. Janssens, J. Dik, W. De Nolf, G. Van der Snickt, Optimization of mobile scanning macro-XRF systems for the in situ investigation of historical paintings, J. Anal. At. Spectrom. 26 (2011) 899–909.

[6] M. Alfeld, J. Vaz Pedroso, M. Van Eikema Hommes, G. Van der Snickt, G. Tauber, J. Blaas, M. Haschke, K. Erler, J. Dik, K. Janssens, A mobile instrument for in-situ scanning macro-XRF investigation of historical paintings', J. Anal. At. Spectrom. 28 (2013) 760–767.

[7] G. Van der Snickt, H. Dubois, J. Sanyova, S. Legrand, A. Coudray, C. Glaude, M. Postec, P. Van Espen, K. Janssens, Large-area elemental imaging reveals Van Eyck's original paint layers on the Ghent altarpiece (1432), rescoping its conservation treatment, Angewandte Chemie 56:17 (2017), 4797-4801

[8] S. Legrand, P. Ricciardi, L. Nodari, K. Janssens, Non-invasive analysis of a 15th century illuminated manuscript fragment: point-based vs imaging spectroscopy, Microchemical Journal 138 (2018) p. 162-172

[9] D. Dungworth, Historic window glass. The use of chemical analysis to date manufacture, Journal of Architectural Conservation 18 (2012) 7–25.

[10] L. W. Adlington, I. C. Freestone, Using handheld pXRF to study medieval stained glass: A methodology using trace elements, MRS Advances 2 (2017), 1785-1800.

[11] W. Meulebroeck, P. Cosyns, K. Baert, H. Wouters, S. Cagno, K. Janssens, Optical spectroscopy as a rapid and low-cost tool for the first-line analysis of glass artefacts: a step-by-step plan for Roman green glass, Journal of Archaeological Science 38 (2011), 2387-2398

[12] W. Meulebroeck, H. Wouters, K. Nys, H. Thienpont, Authenticity screening of stained glasses, Scientific Reports 6 (2016), Article number: 37726

[13] D.W, Ball, The basics of spectroscopy. SPIE Optical Engineering Press (2001).

[14] A. Ceglia et al, Light through glass: The spectrum of Late Antique glass from Cyprus. J. Archaeol. Sci. Reports 7, (2016).

[15] H. Scholze, Glass Nature, Structure, and Properties. Springer-Verlag (1991).

[16] A. Ceglia, G. Nuyts, W. Meulebroeck, S. Cagno, A. Silvestri, A. Zoleo, K. Nys, K. Janssens, H. Thienpont, H. Terryn, Iron speciation in soda lime silica glass: a comparison of XANES and UV-vis-NIR spectroscopy, Journal of Analytical Atomic Spectrometry 30 (2015), 1552-1561

[17] A. Ceglia, Unravelling Technology and Distribution of Ancient Glass by X-Ray and UV-Vis-NIR Absorption Spectroscopy, PhD thesis at the VUB (2015)

[18] Ph. Colomban, A. Tournie, L. Bellot-Gurlet, J. Raman Spectrosc. 37 (2006), 841

[19] Ph. Colomban, J. Non-Cryst. Solids 323 (2003)

[20] A. Rousaki, A. Coccato, C. Verhaeghe, B. Clist, K. Bostoen, P. Vandenabeele, L. Moens, Appl. Phys. A 2016, 70, 79

[21] P. Ricciardi, Ph. Colomban, A. Tournie, M. Macchiarola, N. Ayed, J. Archaeol. Sci. 36 (2009), 2551

[22] P. Ricciardi, Ph. Colomban, A. Tournié, V. Milande, J. Raman Spectrosc. 40 (2009), 604

[23] Ph. Colomban, A. Tournie, J. Cult. Herit. 8 (2007), 242

[24] K. Mouhoubi, J.L. Bodnar, J.M. Vallet, V. Detalle, Follow-up of restoration of works of art of the patrimony by infrared thermography, in: Optics for Arts, Architecture, and Archaeology VII, International Society for Optics and Photonics (2019) 110581E

[25] Y. Yao, S. Sfarra, S. Lagüela, C. Ibarra-Castanedo, J.-Y. Wu, X.P.V. Maldague, D. Ambrosini, Active thermography testing and data analysis for the state of conservation of panel paintings, International Journal of Thermal Sciences. 126 (2018) 143–151

[26] F. Micheletti, J. Orsilli, J. Melada, M. Gargano, N. Ludwig, L. Bonizzoni, The role of IRT in the archaeometric study of ancient glass through XRF and FORS, Microchemical Journal 153 (2020), 104388

[27] T. Palomar, F. Agua, M. Gómez-Heras, Comparative assessment of stained-glass windows materials by infrared thermography, International Journal of Applied Glass Science. 9 (2018) 530–539

[28] T. Palomar, C. Machado, F. Agua, M. Gómez-Heras, Thermographic analysis of glasses, enamels and grisailles from stained glass windows, in: Proceedings of the 5th GLASSAC International Conference, NOVA.FCT Editorial, Caparica, Portugal (2017), 94–97.

[29] C. Machado, A. Machado, T. Palomar, L.C. Alves, M. Vilarigues, Debitus grisailles for stained glass conservation: an analytical study, Cons. Património. (2019)

[30] T. Palomar, M. Silva, M. Vilarigues, I. Pombo Cardoso, D. Giovannacci, Impact of solar radiation and environmental temperature on Art Nouveau glass windows, Heritage Science. 7 (2019) 82

[31] J. Kleinmanns, 1997, Denkmalpflege der Zukunft, Fraunhofer IRB Verlag, Stuttgart, Germany

[32] D. Hutsebaut, P. Vandenabeele, L. Moens, Analyst 130 (2005), 1204

[33] R. L. McCreery, Raman Spectroscopy for Chemical Analysis, John Wiley & Sons, New York (2000)

[34] M. Hillen, S. Legrand, Y. Dirkx, K. Janssens, G. Van der Snickt, J. Caen, G. Steenackers, Cluster Analysis of IR Thermography Data for Differentiating Glass Types in Historical Leaded-glass Windows, Appl. Sci., submitted (2020)

[35] E. D'Accardi, D. Palumbo, R. Tamborrino, U. Galietti, Quantitative analysis of thermographic data through different algorithms, Procedia Structural Integrity. 8 (2018) 354–367

[36] G. Giorleo, C. Meola, Comparison between pulsed and modulated thermography in glass–epoxy laminates, NDT & E International. 35 (2002) 287–292

[37] F.J. Madruga, C. Ibarra-Castanedo, O.M. Conde, J.M. López-Higuera, X. Maldague, Infrared thermography processing based on higher-order statistics, NDT & E International. 43 (2010) 661–666

[38] FLIR X6000sc Series,
http://www.flirmedia.com/MMC/THG/Brochures/RND_088/RND_088_US.pdf

[39] G. Nuyts, S. Cagno, S. Bugani, K. Janssens, Micro-XANES study on Mn browning: use of quantitative valence state maps, Journal of Analytical Atomic Spectrometry 30 (2015), 642-650

[40] M. Schreiner, Glass of the past: The degradation and deterioration of medieval glass artifacts, Microchimica Acta, 104 (1991), 255-264

[41] R. Arletti, S. Quartieri, I.C. Freestone, A XANES study of chromophores in archaeological glass, Applied Physics A: Materials Science and Processing, 111 (2013), 99-108

[42] J. Kunicki-Goldfinger, L. Kierzek, P. Dzierżanowski, A.J. Kasrzak, Central European crystal glass of the first half of the eighteenth century. In: Annales du 16e Congrès de l'Association Internationale pour l'Histoire du Verre. Nottingham: AIHV (2005), 258–262.

[43] C.F. Partington, The British Cyclopaedia of the Arts, Glass, page 605-606, 1838

[44] C.R. Bamford, Colour generation and control in glass. (Elsevier Scientific Publishing Group, 1977).

[45] W. Meulebroeck, H. Wouters, K. Baert, A. Ceglia, H. Terryn, K. Nys, H. Thienpont, Optical spectroscopy applied to the analysis of medieval and post-medieval plain flat glass fragments excavated in Belgium, Proceedings of SPIE 7726 (2010) 77261E-1

[46] W. Meulebroeck et al. 800 Years of FENESTRAtion History. Flat Glass and Windows in Federal Scientific Institutes. In Madeleine Manderyck, Isabelle Lecocq Bemden, Yvette Vanden, Stained Glass in the 17th Century. Continuity, Invention, Twilight. - 29th International Colloquium of the Corpus Vitrearum, Anvers, July 2nd-6th 2018, Antwerpen/Brussels (2018) 169–72.

Table 1. The four glass groups identified in the window by MA-XRF, and their XRF intensities (mean ± standard deviation) for seven discriminating elements. Intensities were calculated by fitting the average spectrum of all pixel spectra in a group, leaving out at least one pixel at the sides to avoid erroneous attribution due to the lead cames. The reader should refer to Figure 13 for pane locations and group colors.

Groups	Number of panes	K intensity	Ca intensity	Mn intensity	Fe intensity	As intensity	Sr intensity	Pb intensity	K/Ca ratio	Tentative classification
Group 1 (*yellow*)	18	680 ± 40	7000 ± 100	3220 ± 60	2010 ± 60	550 ± 60	570 ± 40	400 ± 80	0.10	>18th century HLLA, or mixed alkali/soda glass with high K impurities
Group 2 (*blue*)	2	630 ± 40	7400 ± 100	2700 ± 60	2320 ± 60	860 ± 60	720 ± 40	460 ± 80	0.09	>18th century HLLA, or mixed alkali/soda glass with high K impurities
Group 3 (*green*)	3	1790 ± 60	5400 ± 100	870 ± 40	4410 ± 70	10 ± 60	420 ± 40	620 ± 80	0.33	HLLA or mixed alkali glass, possibly the window's original 17th century glass
Group 4 (*red*)	2	520 ± 30	8100 ± 100	1620 ± 50	1940 ± 50	10 ± 60	480 ± 40	320 ± 80	0.06	Unclear

Table 2. Glass groups identified by UV-Vis-NIR absorption spectroscopy. The reader should refer to Figure 13 for pane locations and group colors.

Groups	Number of panes	Tentative classification	References
Group 1 (*yellow*)	18	HLLA or mixed-alkali glass. Impurities such as iron and cobalt.	Comparable to Middelburg HLLA Group II [45]

Group 2 (*blue*)	2	HLLA or mixed-alkali glass. High content of impurities such as iron, cobalt. One piece is more altered than the others.	Comparable to Bruges and Middelburg HLLA Group III [45]
Group 3 (*green*)	3	HLLA or mixed-alkali glass. Impurities such as iron and cobalt both in lower quantities than in group 1. Probably the same type of glass than group 1 but could correspond to a different batch.	Comparable to Middelburg HLLA Group II [45]
Group 4 (*red*)	2	Not a pure glass, presence of high iron impurities.	No published comparison yet
Group 5 (*purple*)	1	Not a pure glass, presence of high iron impurities. Probably the same or similar type of glass than group 4.	No published comparison yet

Figure 1. The exterior side of the leaded window (a) in transmitted light and (b) in reflected light.

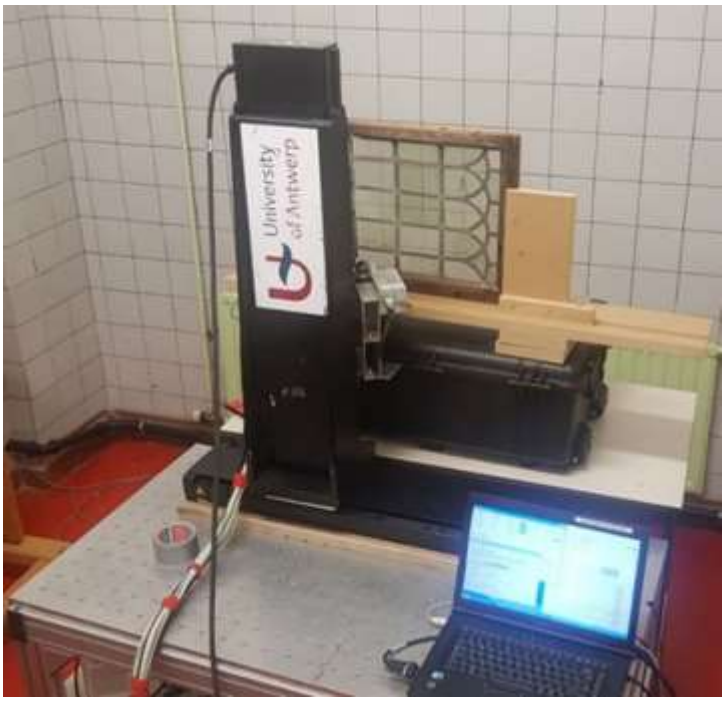

Figure 2 The MA-XRF scanning setup, namely instrument version I, built within the AXES group of the University of Antwerp.

Figure 3. The UV-Vis-NIR setup employed in this study.

Figure 4. The portable EZRaman-I dual spectrometer. Two different excitation probe heads are attached to the articulated arm for easy positioning and focusing of the beam. Credits: Debbie Lauwers.

Figure 5. Transmission set-up for the IRT measurements with the back of the window heated. In reflection mode, the window is heated from the front side with the lamps alongside the camera while maintaining the same distances and angles with respect to the window.

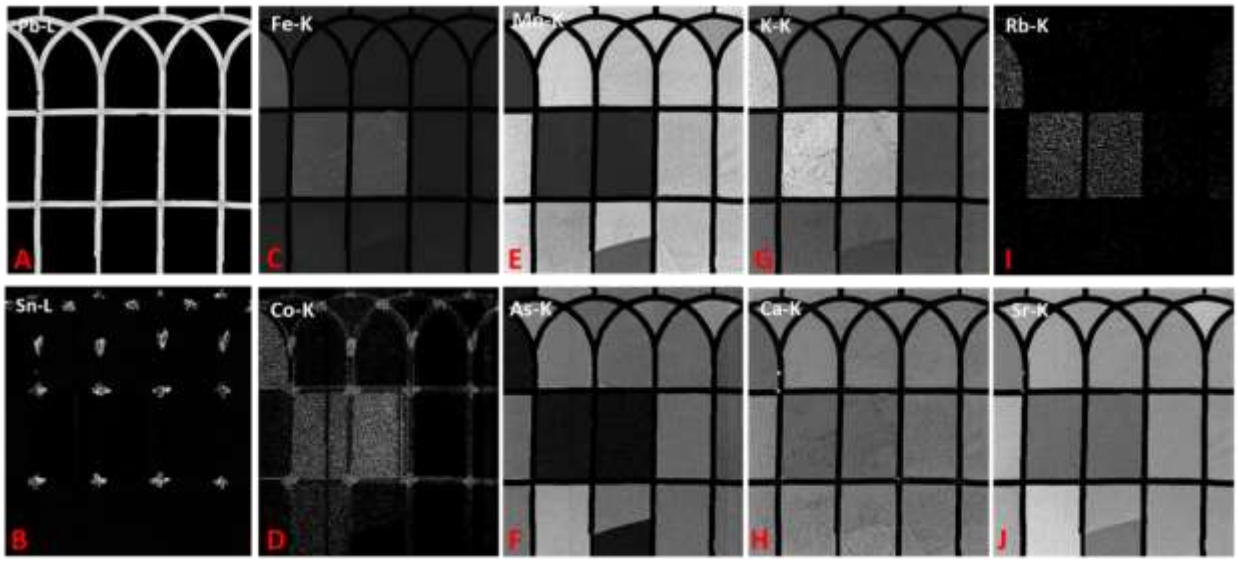

Figure 6 MA-XRF results shown as fluorescence distribution maps of the window: (A) Pb-L and (B) Sn-L showing the lead came network and Sn-containing soldering alloy; the colorants and decolorizers emerge in (C) Fe-K and (D) Mn-K, (E) Co-K and (F) As-K; the network modifiers in (G) K-K and (H) Ca-K, with related trace elements (I) Rb-K and (J) Sr-K, respectively.

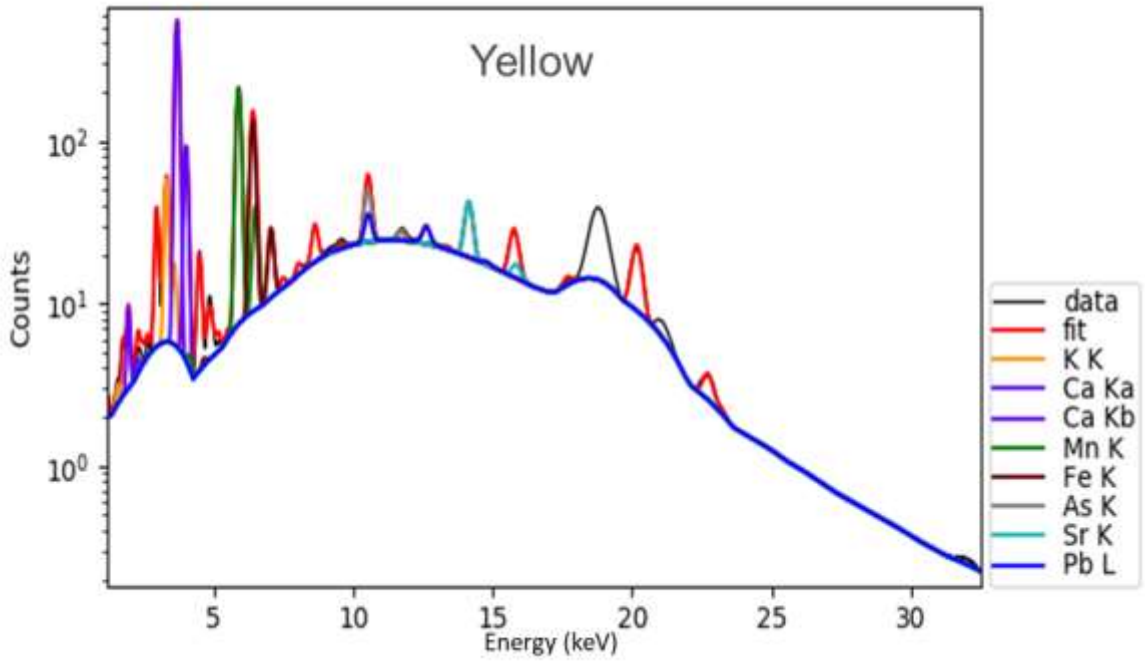

Figure 7. Fitted average MA-XRF spectrum of all spectra recorded in the panes of Group 1 (*yellow*) with peak attributions. The average spectra of the other glass groups are shown in the Supplementary Information.

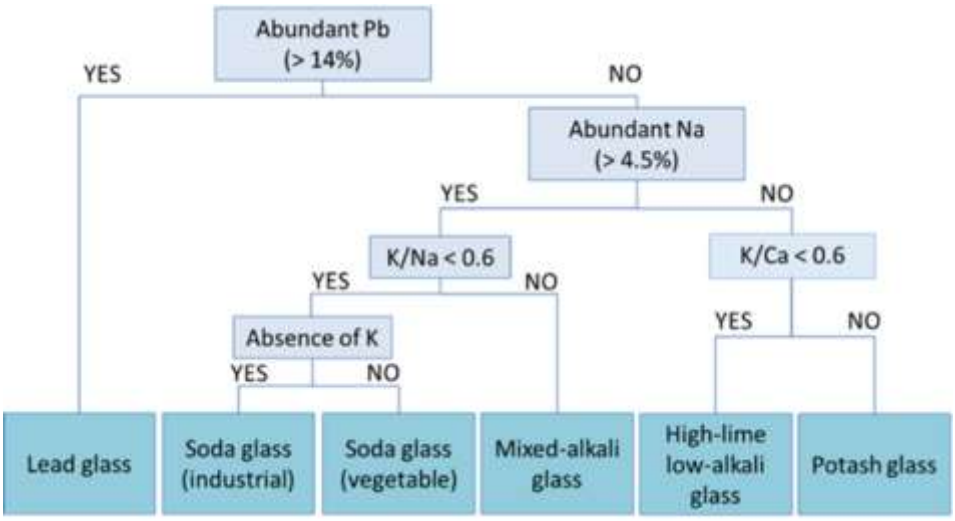

Figure 8. Glass types occurring in the Low Countries and surrounding areas from the 16th century to present [1] (further edited in [4]).

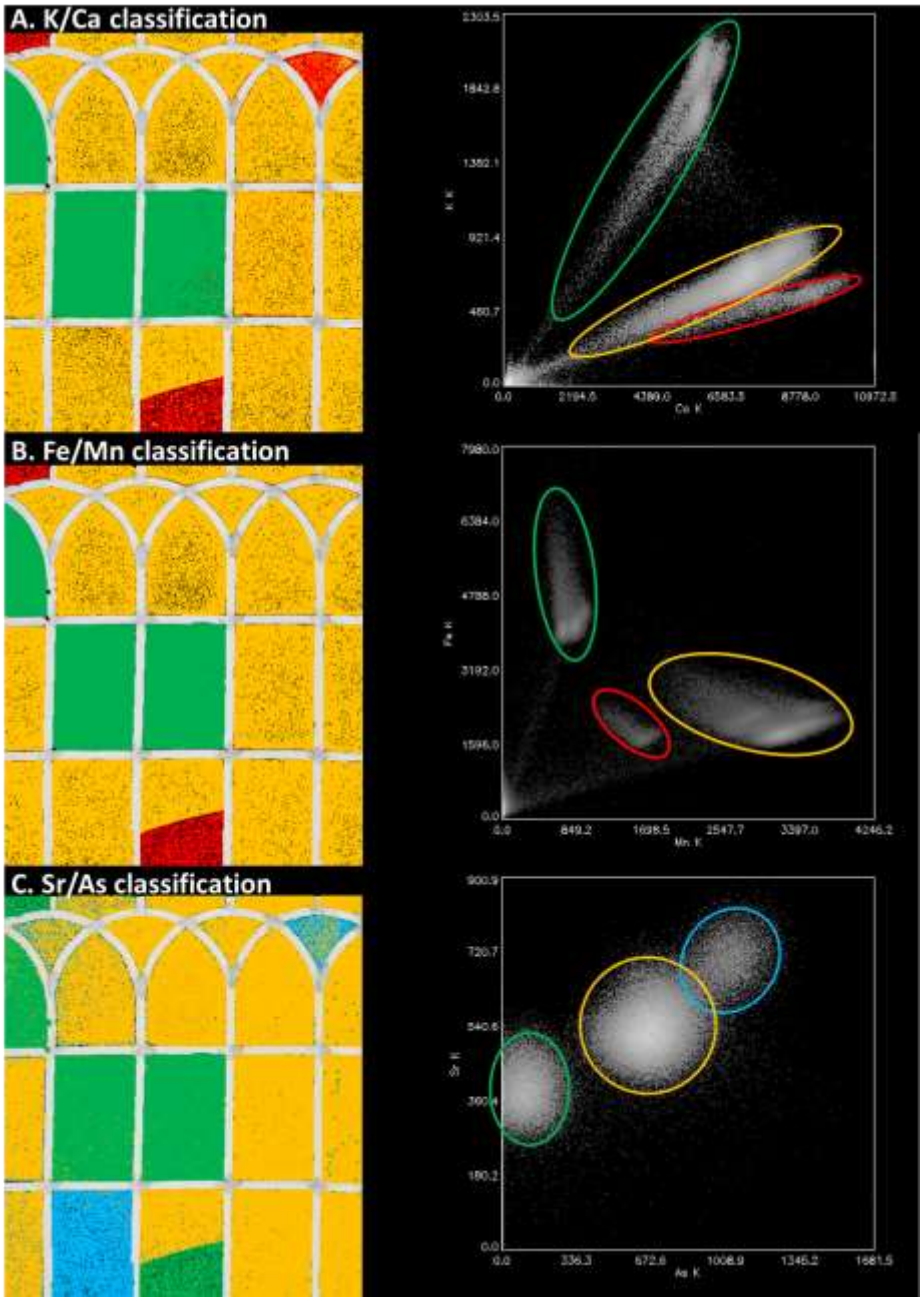

Figure 9: MA-XRF elemental scatter plots (right) and associated false color maps (left) of the window: (A) K/Ca, (B) Fe/Mn, (C) Sr/As.

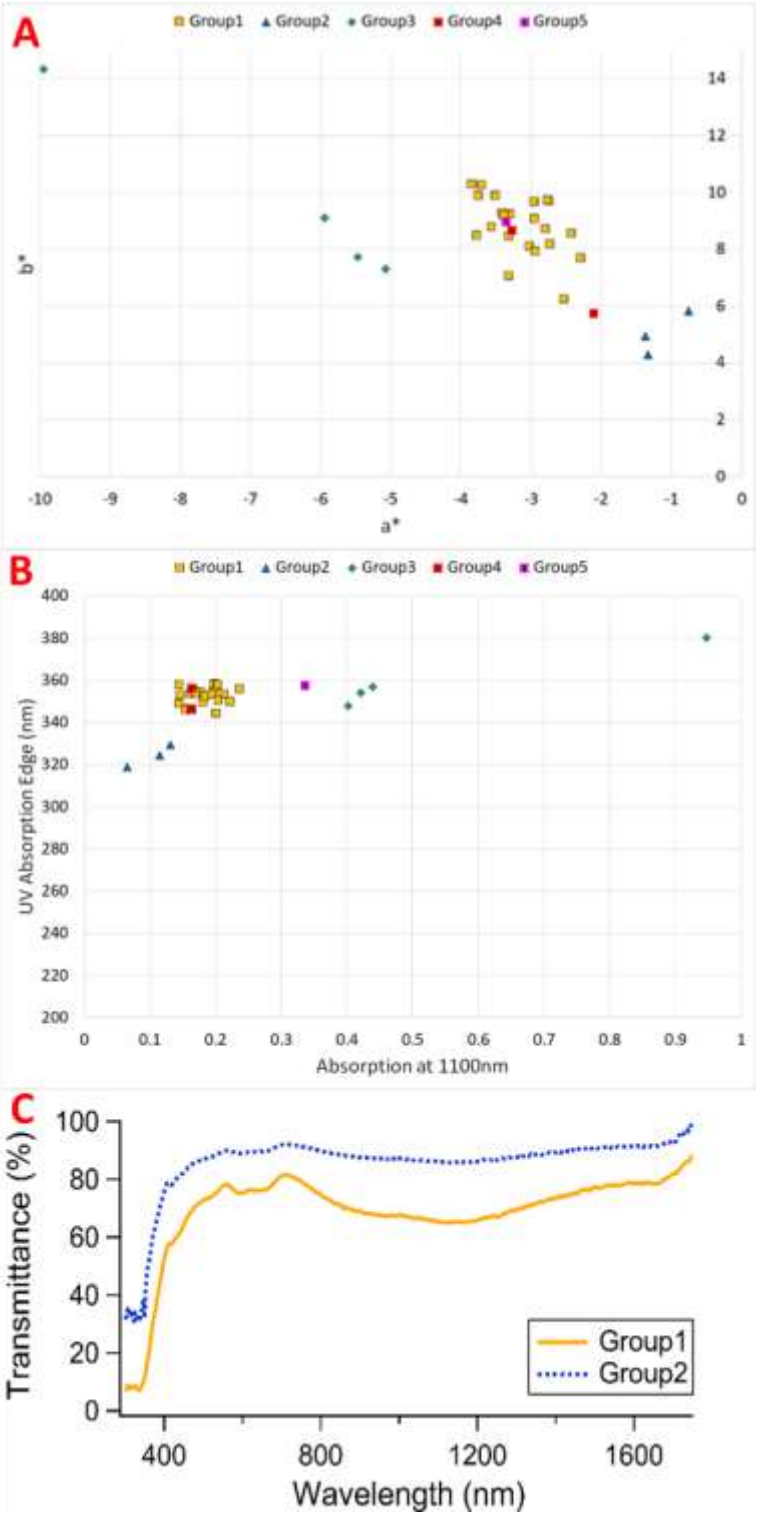

Figure 10 A-C. UV-Vis-NIR shown as (A) CIE L*a*b* color space, a* and b* color coordinates for the illuminant D65 at the measured spots of the window; (B) UV absorption edge and absorption at 1100 nm at the measured spots of the window; (C) Transmittance spectra of two glass groups, showing characteristic absorption bands due to presence of Co.

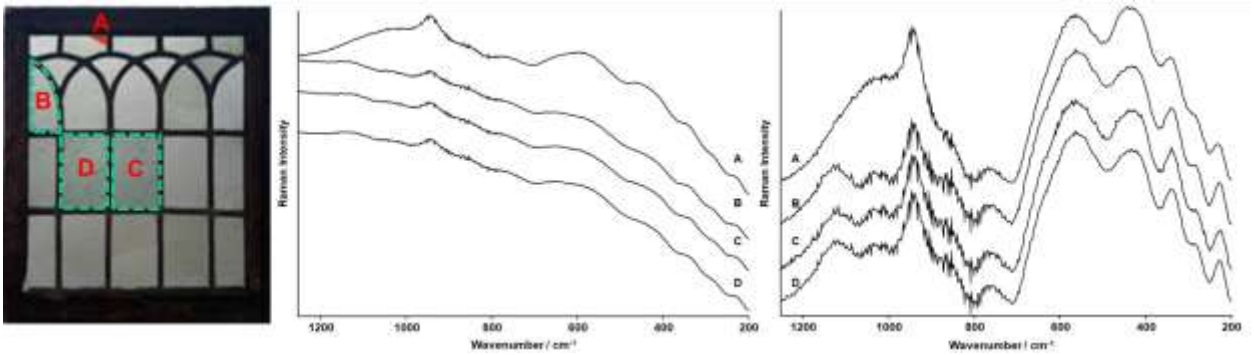

Figure 11. From left to right: locations where the Raman spectra shown on the right were collected; raw Raman spectra collected at the four locations; linear baseline spectra collected at the four locations.

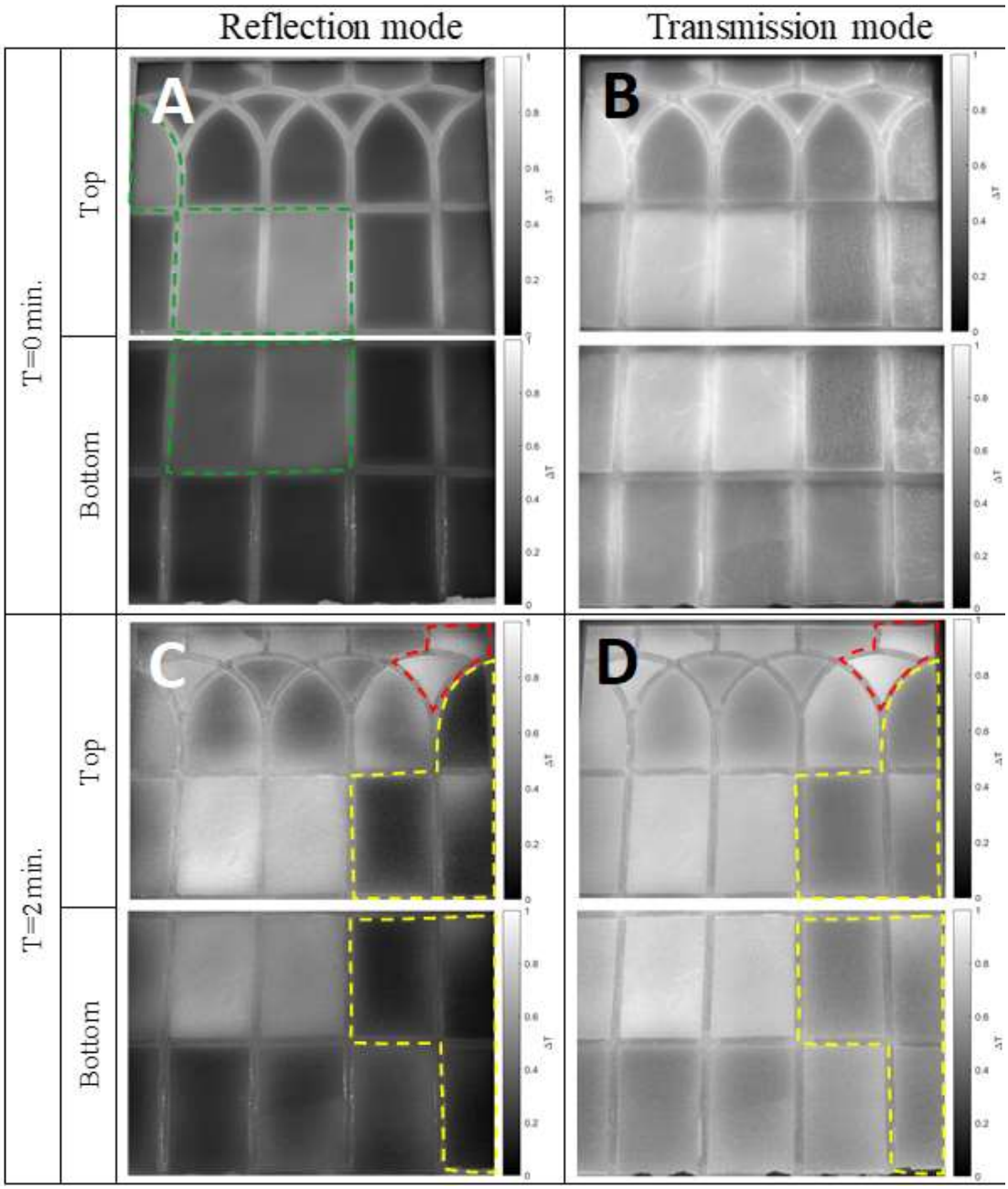

Figure 12 A-D. Active IRT results: separate thermograms were recorded on the upper and lower parts of the window to optimize spatial resolution, shown in top and bottom rows respectively. The thermograms have one overlapping register of glass panes. Experiments were performed in reflection and transmission mode, before cooling (t=0) and during cooling (t=2 min): (A) Reflected IRT, t=0; (B) Transmitted IRT, t=0; (C) Reflected IRT, t=2 min; (D) Transmitted IRT, t=2 min

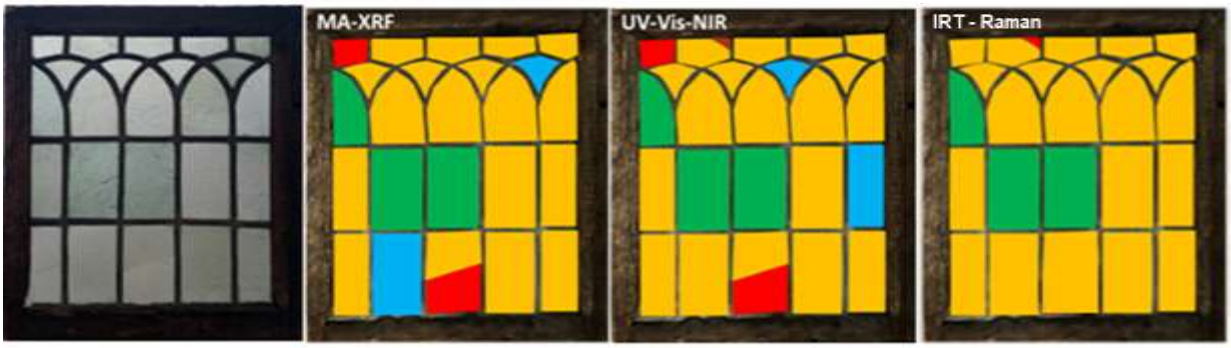

Figure 13. From left to right: glass window in transmitted light and classification of glass panes based on MA-XRF, UV-Vis-NIR spectroscopy, and IRT combined with Raman spectroscopy results). NB: With Raman spectroscopy only the *green* and the *red* panes could be positively identified, while the *yellow* group was identified negatively, based on the common excess fluorescence.